Research Article Vol. 32, No. 5 / 26 Feb 2024 / Optics Express 7865
Optics EXPRESS

# SESAM mode-locked Yb:$GdScO_3$ laser

JIE GUO,[1] SHANMING LI,[2] CHENGCHUN ZHAO,[2] YIN HANG,[2] HUANG-JUN ZENG,[3] ZHANG-LANG LIN,[3] GE ZHANG,[3] GHASSEN ZIN ELABEDINE,[4] XAVIER MATEOS,[4] PAVEL LOIKO,[5] VALENTIN PETROV,[6] WEIDONG CHEN,[3,6] AND XIAOYAN LIANG[1,*]

[1]*State Key Laboratory of High Field Laser Physics, Shanghai Institute of Optics and Fine Mechanics, Chinese Academy of Sciences, 201800 Shanghai, China*
[2]*Advanced Laser and Optoelectronic Functional Materials Department, Shanghai Institute of Optics and Fine Mechanics, Chinese Academy of Sciences, 201800 Shanghai, China*
[3]*Fujian Institute of Research on the Structure of Matter, Chinese Academy of Sciences, 350002 Fuzhou, China*
[4]*Universitat Rovira i Virgili, URV, Física i Cristal Lografia de Materials (FiCMA), Marcel lí Domingo 1, 43007 Tarragona, Spain*
[5]*Centre de Recherche sur les Ions, les Matériaux et la Photonique (CIMAP), UMR 6252 CEA-CNRS-ENSICAEN, Université de Caen, 6 Boulevard Maréchal Juin, 14050 Caen Cedex 4, France*
[6]*Max Born Institute for Nonlinear Optics and Short Pulse Spectroscopy, Max-Born-Str. 2a, 12489 Berlin, Germany*
[*]*liangxy@siom.ac.cn*

**Abstract:** We report on the investigation of continuous-wave (CW) and SEmiconductor Saturable Absorber Mirror (SESAM) mode-locked operation of a Yb:$GdScO_3$ laser. Using a single-transverse-mode, fiber-coupled InGaAs laser diode at 976 nm as a pump source, the Yb:$GdScO_3$ laser delivers 343 mW output power at 1062 nm in the CW regime, which corresponds to a slope efficiency of 52%. Continuous tuning is possible across a wavelength range of 84 nm (1027–1111 nm). Using a commercial SESAM to initiate mode-locking and stabilize soliton-type pulse shaping, the Yb:$GdScO_3$ laser produces pulses as short as 42 fs at 1065.9 nm, with an average output power of 40 mW at 66.89 MHz. To the best of our knowledge, this is the first demonstration of passively mode-locking with Yb:$GdScO_3$ crystal.

© 2024 Optica Publishing Group under the terms of the Optica Open Access Publishing Agreement

## 1. Introduction

Rare-earth orthoscandates with the chemical formula $REScO_3$, where RE is a rare-earth element such as Y or Ln = La - Tm can crystallize with the orthorhombic $GeFeO_3$-type crystal symmetry (sp. gr. $D_{2h}^{16} - P_{mma}$ or $P_{bnm}$) [1] which is a distorted modification of the cubic perovskite structure known from the established $YAlO_3$ (YAP) laser host crystal [2]. The heavier of them (Y and Ln = Er – Tm) do not form perovskites at ambient conditions [3] while some of the perovskites melt congruently and therefore can be grown by the conventional Czochralski (Cz) technique resulting in large volume and high optical quality single crystals for Ln = Nd - Dy [4]. Gadolinium scandate, $GdScO_3$, with lattice constants $a = 5.7499$ Å, $b = 7.9345$ Å and $c = 5.4862$ Å (sp. gr. $P_{nma}$) [3], being optically passive, is an important representative of this family that is suitable as a laser host crystal [4]. It exhibits relatively low phonon energies among oxide host crystals, similar to the related cubic sesquioxides [5]. The linear thermal expansion coefficients of $GdScO_3$ amount to $\alpha_a = 6.7$, $\alpha_b = 11.5$ and $\alpha_c = 14.5 \times 10^{-6}\,K^{-1}$ [6].

The first investigation on $GdScO_3$ as a laser host material focused on $Nd^{3+}$ doping [7,8]. The $GdScO_3$ crystal is optically biaxial and the average refractive index at 1064 nm was estimated to be 2.0710 [8]. Its intrinsic birefringence leads to naturally polarized and suppresses thermal induced depolarization losses. More recently, the $GdScO_3$ crystal has been studied as a host matrix for other laser-active RE dopants such as $Dy^{3+}$ [9,10], $Tm^{3+}$ [11–14], $Er^{3+}$ [15,16], $Ho^{3+}$

#512293 https://doi.org/10.1364/OE.512293
Journal © 2024 Received 15 Nov 2023; revised 20 Jan 2024; accepted 31 Jan 2024; published 20 Feb 2024

Optics EXPRESS

[17], $Pr^{3+}$ [18,19] and $Yb^{3+}$ [20,21]. The dopant ions replace the host-forming $Gd^{3+}$ cations in sites with VIII-fold oxygen coordination and large variation of metal-to-oxygen bond lengths and angles. In contrast to YAP, doped $GdScO_3$ exhibits rather broad absorption and emission bands at room temperature. The nature of the exact spectral broadening mechanism is still unclear. Laser operation has been demonstrated so far for $Nd^{3+}$ [7,22], $Er^{3+}$ [15,16], $Tm^{3+}$ [11,12] and $Yb^{3+}$ [21] doped $GdScO_3$.

For example, $GdScO_3$ doped with $Tm^{3+}$ exhibits untypically broad and smooth gain profiles, with a spectral bandwidth exceeding 200 nm. This unique feature renders it highly suitable for a wide range of applications, including tunable lasers and femtosecond mode-locked (ML) laser operation. In the continuous-wave (CW) regime, pumping by a single-transverse-mode Raman shifted Er-fiber laser at 1700 nm, a tuning range of 321.3 nm was achieved with Tm:$GdScO_3$ laser using a Lyot filter [23]. Employing a SEmiconductor Saturable Absorber Mirror (SESAM), the ML Tm:$GdScO_3$ laser delivered pulses as short as 44 fs at 2042 nm with an average output power of 188 mW [24].

For laser emission near 1 µm, Yb-doped materials benefit from a simple energy-level scheme of the $Yb^{3+}$ ion consisting of just two multiplets ($^2F_{7/2}$: ground-state, $^2F_{5/2}$: excited-state). Combined with efficient in-band pumping by commercial high-power InGaAs diode lasers emitting at 980 nm this enables higher output powers at weaker heat load as compared to $Nd^{3+}$ lasers. $Yb^{3+}$-doped $GdScO_3$ is attractive for ~1 µm lasers due to its good thermo-mechanical and spectroscopic properties. The thermal conductivity for a 2.22 at.% $Yb^{3+}$-doped $GdScO_3$ is $\kappa_b = 5.54$ and $\kappa_c = 5.33$ W/mK at 50°C [21]. The room-temperature fluorescence lifetime of the upper laser level ($^2F_{5/2}$) of $Yb^{3+}$ in $GdScO_3$ was measured to be 551 µs [21]. Pumping with a fiber-coupled multi-mode diode laser at 976 nm, the maximum CW output power of the Yb:$GdScO_3$ laser reached 13.45 W at 1063.9 nm with an optical efficiency of 63.3% [21].

Given the aforementioned characteristics and previous CW laser studies, Yb:$GdScO_3$ appears highly promising for sub-100 fs passively ML lasers. We are not aware of any previous ultrashort pulse generation experiments performed with Yb:$GdScO_3$ crystals. In this study, we present diode-pumped, passively ML operation of Yb:$GdScO_3$, achieving pulse duration below 50 fs.

## 2. Experimental setup

### 2.1. Crystal growth and spectroscopy

The Yb:$GdScO_3$ crystal employed was grown by the conventional Cz method, using RE sesquioxide powders, $Gd_2O_3$, $Sc_2O_3$ and $Yb_2O_3$, with a purity level of 99.99%. The polycrystalline precursor for the crystal growth was synthesized by a solid-state reaction. For this purpose, the raw materials were weighed assuming a stoichiometric composition with a nominal Yb content of 5 at.%. After mixing them for 10 hours to achieve homogeneity, the mixture was pressed into disks and subjected to a 10-hour heating process in air at 1500°C. The growth was carried in argon atmosphere using an iridium crucible with $ZrO_2$ as an isolator. The rotation speed and the pulling rate were 10 rpm and 1.5 mm/h, respectively. The as grown bulk was gradually cooled to room temperature at a rate of 80°C/h. The resulting boule had dimensions of $\Phi 40 \times 30$ mm$^3$ and exhibited a yellow tinge, as shown in Fig. 1.

The actual crystal composition was measured by the inductively coupled plasma atomic emission spectrometry (ICP-AES) yielding an $Yb^{3+}$ doping level of 4.1 at.% (ion density: $N_{Yb}$ $=6.3 \times 10^{20}$ cm$^{-3}$, segregation coefficient for Yb incorporation in $GdScO_3$: $K_{Yb} = 0.82$).

Yb:$GdScO_3$ samples can be oriented in the crystallographic frame $\boldsymbol{a}$, $\boldsymbol{b}$, $\boldsymbol{c}$ because for orthorhombic symmetry it coincides with the frame of the optical ellipsoid. According to the quasi-three-level Yb laser scheme with reabsorption ($^2F_{5/2} \leftrightarrow {}^2F_{7/2}$), the potential gain bandwidth for tunable or ML operation and the central wavelength can be estimated by calculating the gain cross-sections, $\sigma_{gain} = \beta\sigma_{SE} - (1-\beta)\sigma_{abs}$, where $\beta = N_2/N_{Yb}$ denotes the inversion ratio, i.e., the ratio of the number of ions excited to the upper laser level $N_2(^2F_{5/2})$ to the total $Yb^{3+}$

Optics EXPRESS

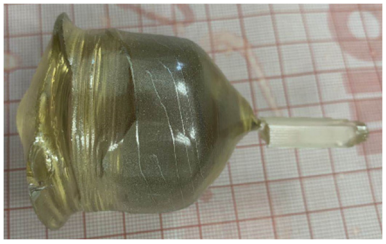

**Fig. 1.** A photograph of the as-grown 5 at.% Yb:$GdScO_3$ crystal.

ion density. The broad, smooth and flat gain spectra of Yb:$GdScO_3$ shown in Fig. 2 for light polarization $\boldsymbol{E} \parallel \boldsymbol{c}$ and inversion ratios in the 0.05–0.3 range indicate a high potential for broad wavelength tuning and sub-50 fs pulse generation in passively ML lasers.

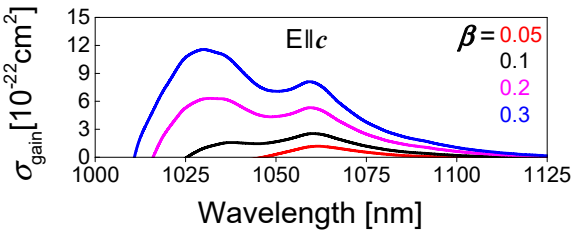


**Fig. 2.** Calculated gain cross-section, $\sigma_{gain} = \beta\sigma_{SE} - (1-\beta)\sigma_{abs}$, spectra of Yb:$GdScO_3$ for different inversion ratios $\beta = N_2/N_{Yb}$ and light polarization $\boldsymbol{E} \parallel \boldsymbol{c}$.

### 2.2. Laser set-up

The laser element used was 3-mm thick along the $\boldsymbol{b}$-axis ($\boldsymbol{b}$-cut) and had a rectangular shape with an aperture of 4 mm ($\boldsymbol{a}$) × 4 mm ($\boldsymbol{c}$). The two faces were polished to laser-grade quality and left uncoated sample was inclined at Brewster's angle for polarization along the $\boldsymbol{c}$-axis ($\boldsymbol{E} \parallel \boldsymbol{c}$). Figure 3 shows the experimental configuration of the Yb:$GdScO_3$ laser.

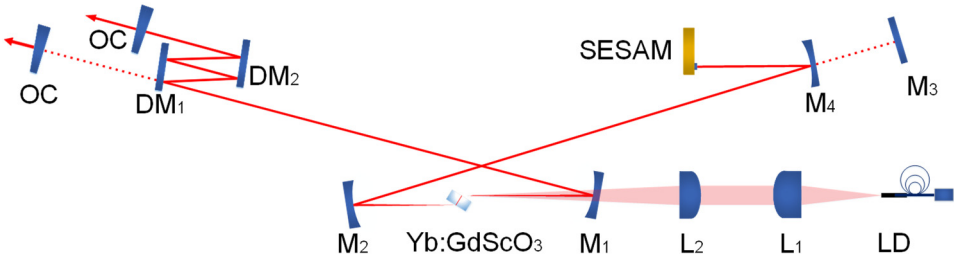


**Fig. 3.** Experimental setup of the Yb:$GdScO_3$ laser. LD: fiber-coupled 976-nm laser diode; $L_1$: aspherical lens; $L_2$: spherical focusing lens; $M_1$, $M_2$ and $M_4$: concave mirrors; $M_3$: flat rear mirror for CW laser operation; $DM_1$ and $DM_2$: flat dispersive mirrors; OC: output coupler; SESAM: SEmiconductor Saturable Absorber Mirror.

An X-folded linear resonator with astigmatically compensation was employed to access the CW and ML laser performance. The Yb:$GdScO_3$ crystal was placed between two dichroic concave mirrors, $M_1$ and $M_2$, both with a radius of curvature (RoC) of -100 mm. It was mounted in a copper holder but no active cooling was applied. The pump source was a single-transverse-mode,

Optics EXPRESS

fiber-coupled InGaAs laser diode (Connet, VENUS) with an almost diffraction-limited spatial intensity distribution (beam propagation factor $M^2 = 1.07$). Its emission wavelength was locked to 976 nm resulting in a spectral linewidth (full width at half maximum, FWHM) of 0.2 nm. The unpolarized pump source provided a maximum incident power on the crystal of 1.3 W. The pump beam was reimaged into the laser crystal using an aspherical collimating lens $L_1$ with a focal length of 26 mm and a spherical focusing lens $L_2$ with a focal length of 75 mm. A beam waist (radius) of 13.7 µm × 16.8 µm in the sagittal and tangential planes, respectively, was estimated in the position of the crystal.

The CW Yb:$GdScO_3$ laser utilized a four-mirror cavity with a flat end mirror $M_3$ and a flat output coupler (OC). Different OC transmission $T_{OC}$ ranging from 1 to 7.5% was used. The cavity mode size in the crystal can be calculated by the ABCD formalism. The result for the beam radii in the sagittal and tangential planes was 19 µm × 41 µm, respectively. The dependence of the single-pass pump absorption on $T_{OC}$ measured under lasing conditions was weak, with values in the 63.3% to 64.6% range.

A commercial SESAM (BATOP, GmbH) was employed to initiate and stabilize passive mode-locking of the Yb:$GdScO_3$ laser. Its modulation depth of 0.9% was 1.5 higher than the nonsaturable losses of ~0.6% measured near 1 µm whereas the specified recovery time amounted to 10 ps. To effectively bleach the SESAM, a beam waist on it was created by replacing the flat end mirror $M_3$ by a concave mirror $M_4$ (RoC = -100 mm). This secondary beam waist had a radius of 40 µm. The resonator material dispersion was compensated by inserting two flat dispersive mirrors (DMs) in the cavity arm containing the OC which simultaneously facilitates soliton-like pulse shaping in the presence of self-phase modulation (SPM) due to the crystal Kerr nonlinearity. They exhibited a negative group delay dispersion (GDD) of -250 $fs^2$ per bounce. The pulse repetition rate calculated from the physical cavity length of the ML (2.24 m) is roughly 66.9 MHz.

## 3. Continuous-wave laser operation

The maximum output power of the CW Yb:$GdScO_3$ laser reached 343 mW at 1062 nm at an absorbed pump power of 849 mW using a 1.6% OC. The laser threshold in this case was 202 mW and the slope efficiency 52%, as illustrated in Fig. 4(a). For the maximum $T_{OC} = 7.5\%$ the slope efficiency was only slightly higher (52.9%) but the output power dropped to 197 mW. The laser

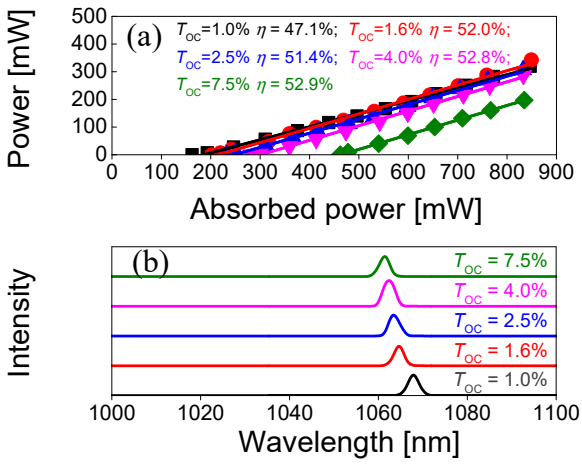


**Fig. 4.** CW diode-pumped Yb:$GdScO_3$ laser: (a) Input-output dependence versus $T_{OC}$, $\eta$ – slope efficiency; (b) Typical laser emission spectra, laser polarization: $\boldsymbol{E} \parallel \boldsymbol{c}$.

Optics EXPRESS

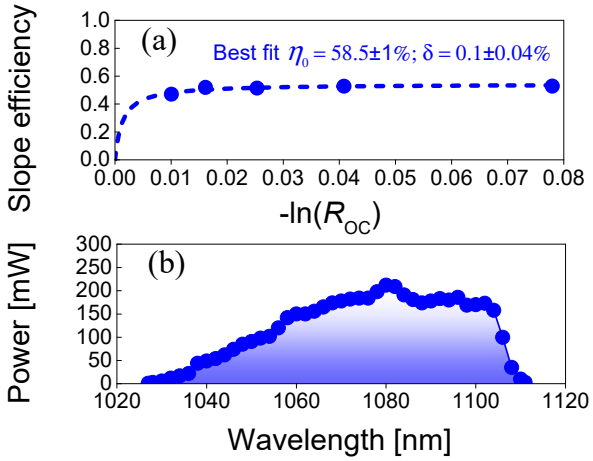


**Fig. 5.** CW diode-pumped Yb:$GdScO_3$ laser: (a) Caird analysis for assessing the total round-trip cavity losses $\delta$ and intrinsic slope efficiency $\eta_0$; (b) Tuning performance using a Lyot filter for $T_{OC} = 0.4\%$. The output polarization is $\boldsymbol{E} \,||\, \boldsymbol{c}$.

threshold gradually increased with the OC transmission from 162 mW ($T_{OC} = 1\%$) to 462 mW ($T_{OC} = 7.5\%$). In the same time, the emission wavelength of the laser experienced a monotonic blue-shift in the 1061–1068 nm range, as depicted in Fig. 4(b). This behavior is explained by the reabsorption effect at the laser wavelength, characteristic of quasi-three-level $Yb^{3+}$ lasers.

The total cavity losses (reabsorption losses excluded) were evaluated by the Caird analysis, plotting the experimental laser slope efficiency versus -ln($R_{OC}$) where $R_{OC} = 1 - T_{OC}$ [25]. This gave round-trip cavity losses of $\delta = 0.1 \pm 0.04\%$. The result for the intrinsic slope efficiency $\eta_0$, involving mode-matching and the quantum efficiencies, was 58.5 ± 1%, as shown in Fig. 5(a).

Wavelength tuning of the CW Yb:$GdScO_3$ laser was investigated at the maximum pump level and minimum OC transmission ($T_{OC} = 0.4\%$). The tuning element was a 2-mm thick quartz plate acting as a Lyot filter. It was inserted at Brewster angle close to the OC. The laser supported continuous wavelength tuning from 1027 to 1111 nm, coving a range of 84 nm at the zero-power level, as illustrated in Fig. 5(b).

## 4. Mode-locked laser operation

With the SESAM and two DMs ($DM_1 - DM_2$) providing a total round-trip GDD of -2000 $fs^2$, as shown in Fig. 3, stable and self-starting ML operation of the Yb:$GdScO_3$ laser was readily achieved after a careful cavity alignment. Optimum results were obtained for $T_{OC} = 1.6\%$.

Figure 6 shows the characteristics of the shortest pulses directly generated from the diode-pumped Yb:$GdScO_3$ laser. As can be seen in Fig. 6(a), the optical spectrum was centered at 1065.9 nm with a spectral width of (FWHM) of 31 nm assuming a $sech^2$-dependence. The intensity autocorrelation function recorded using second harmonic generation (SHG) could be also almost perfectly fitted assuming a $sech^2$-shaped pulse temporal profile, as shown in Fig. 6(b). The estimated pulse duration (FWHM intensity) was 42 fs. No satellites or multi-pulsing are seen in the long-scale autocorrelation trace shown in the inset of Fig. 6(b). The resulting time-bandwidth product (TBP) of 0.344, which exceeds only slightly the value for Fourier-transform-limited pulses (0.315), and the excellent fits are strong indications of soliton-like pulse shaping in this ML laser. The shortest pulses from the SESAM ML Yb:$GdScO_3$ laser corresponded to a maximum average output power of 40 mW or a peak power of 12.5 kW. The absorbed pump power in this case amounted to 833 mW. Such relatively low average output

Optics EXPRESS

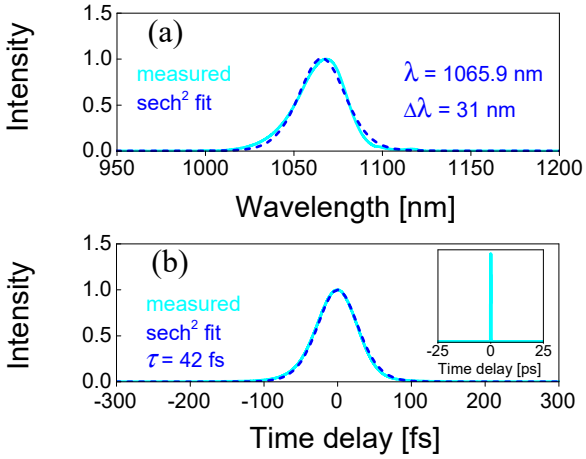


**Fig. 6.** Diode-pumped SESAM ML Yb:$GdScO_3$ laser ($T_{OC} = 1.6\%$): (a) Optical spectrum and (b) intensity autocorrelation (AC) trace. *Inset*: AC trace on a 50 ps time scale.

To ascertain the dominant mode-locking mechanism, we captured the far-field output beam profile of the Yb:$GdScO_3$ laser at 0.6 m from the OC using an infrared (IR) camera. Figure 7 shows them in the CW and ML modes of operation for $T_{OC} = 1.6\%$. In the CW regime, the

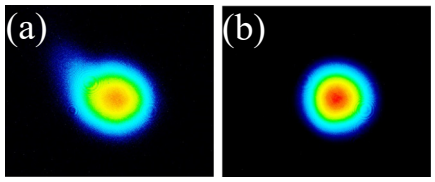


**Fig. 7.** Measured far-field beam profiles of the Yb:$GdScO_3$ laser: (a) CW and (b) ML regimes of operation. $T_{OC} = 1.6\%$.

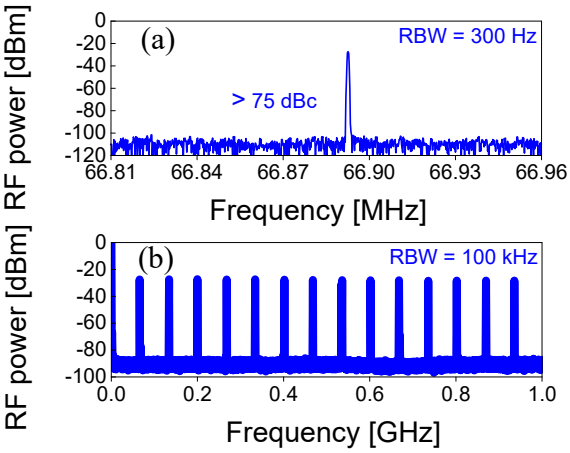


**Fig. 8.** RF spectra of the SESAM ML Yb:$GdScO_3$ laser: (a) Fundamental beat note at ~66.89 MHz measured with a resolution bandwidth (RBW) of 300 Hz, and (b) harmonics recorded on a 1-GHz frequency span with a RBW of 100 kHz.

Optics EXPRESS

laser beam diameter was $1.59 \times 1.55\,mm^2$. Upon initiating mode-locking with the SESAM, the measured beam diameter decreased to $1.39 \times 1.43\,mm^2$. This observation suggests a primary mode-locking mechanism due to soft-aperture Kerr-lensing, stabilized by the SESAM, which can be attributed to the high-brightness of the pump source. However, one cannot rule out some pulse-shaping effect by the SESAM given the rather wide stability zone.

To confirm the stability of the ML Yb:$GdScO_3$ laser, we recorded the radio frequency (RF) spectra for the shortest output pulses in different frequency span ranges. Figure 8(a) shows the fundamental beat note for $T_{OC} = 1.6\%$, located near 66.89 MHz. It exhibits a rather high extinction ratio above carrier of more than 75 dBc and no satellites are seen. Stable single-pulse ML operation free Q-switching instabilities can be also inferred from the uniform harmonics observed over a 1-GHz frequency span, as shown in Fig. 8(b).

## 5. Conclusion

In summary, we achieved sub-50 fs pulse durations from a SESAM ML Yb:$GdScO_3$ laser, using a spatially single-mode, fiber-coupled InGaAs diode laser as a pump source at 976 nm. Employing a commercial SESAM to initiate and stabilize the mode-locking, this laser produced soliton-like pulses as short as 42 fs at 1065.9 nm. The average output power was 40 mW for a pulse repetition frequency of 66.89 MHz. This represents the first demonstration of passively ML operation with the Yb:$GdScO_3$ crystal. Our results indicate that this new material is promising for power scaling and pulse shortening through the application of Kerr-lens mode-locking techniques which we plan for the future experiments.

**Funding.** National Natural Science Foundation of China (62005298, 61975208, 61905247, U21A20508); Sino-German Scientist Cooperation and Exchanges Mobility Program (M-0040); Ministerio de Ciencia e Innovación (MCIN/AEI/10.13039/501100011033, PID2019-108543RB-I00, PID2022-141499OB-I00).

**Acknowledgment.** Xavier Mateos acknowledges the Serra Húnter program.

**Disclosures.** The authors declare no conflicts of interest.

**Data availability.** Data underlying the results presented in this paper are not publicly available at this time but may be obtained from the authors upon reasonable request.

## References

1. J. B. Clark, P. W. Richter, and L. D. Toit, "High-pressure synthesis of $YScO_3$, $HoScO_3$, $ErScO_3$, and $TmScO_3$, and a reevaluation of the lattice constants of the rare earth scandates," J. Solid State Chem. **23**(1-2), 129–134 (1978).
2. R. Diehl and G. Brandt, "Crystal structure refinement of $YAlO_3$, a promising laser material," Mater. Res. Bull. **10**(2), 85–90 (1975).
3. R. P. Liferovich and R. H. Mitchell, "A structural study of ternary lanthanide orthoscandate perovskites," J. Solid State Chem. **177**(6), 2188–2197 (2004).
4. R. Uecker, B. Velickov, D. Klimm, *et al.*, "Properties of rare-earth scandate single crystals (Re = Nd-Dy)," J. Cryst. Growth **310**(10), 2649–2658 (2008).
5. O. Chaix-Pluchery and J. Kreisel, "Raman scattering of perovskite $DyScO_3$ and $GdScO_3$ single crystals," J. Phys.: Condens. Matter **21**(17), 175901 (2009).
6. M. D. Biegalski, J. H. Haeni, S. Trolier-McKinstry, *et al.*, "Thermal expansion of the new perovskite substrates $DyScO_3$ and $GdScO_3$," J. Mater. Res. **20**(4), 952–958 (2005).
7. P. Arsenev, K. Bienert, and R. Sviridova, "Spectral properties of neodymium ions in the lattice of $GdScO_3$ crystals," Phys. Stat. Sol. (a) **9**(2), K103–K104 (1972).
8. S. N. Amanyan, P. A. Arsen'ev, K. S. Bagdasarov, *et al.*, "Synthesis and examination of $GdScO_3$ single crystals activated by $Nd^{3+}$," J. Appl. Spectrosc. **38**(3), 343–348 (1983).
9. F. Peng, W. Liu, J. Luo, *et al.*, "Study of growth, defects and thermal and spectroscopic properties of Dy:$GdScO_3$ and Dy,Tb:$GdScO_3$ as promising 578 nm laser crystals," CrystEngComm **20**(40), 6291–6299 (2018).
10. F. Peng, W. Liu, Q. Zhang, *et al.*, "Growth, structure, and spectroscopic characteristics of a promising yellow laser crystal Dy:$GdScO_3$," J. Lumin. **201**, 176–181 (2018).
11. J. Liu, S. Li, C. Qian, *et al.*, "High-beam-quality 2 µm tunable Tm:$GdScO_3$ laser pumped by a 793 nm laser diode," Laser Phys. Lett. **19**(11), 115801 (2022).
12. S. Li, Q. Fang, Y. Zhang, *et al.*, "2 µm ultrabroad spectra and laser operation of Tm:$GdScO_3$ crystal," Opt. Laser Technol. **143**, 107345 (2021).

Optics EXPRESS


13. Q. Li, J. Dong, Q. Wang, *et al.*, "Growth and spectroscopic properties of $Tm^{3+}$ and $Tb^{3+}$ co-doped $GdScO_3$ crystal," J. Lumin. **230**, 117681 (2021).
14. Q. Li, J. Dong, Q. Wang, *et al.*, "Crystal growth, spectroscopic characteristics, and Judd-Ofelt analysis of Tm:$GdScO_3$," Opt. Mater. **109**, 110298 (2020).
15. W. Hou, Y. Xue, Z. Qin, *et al.*, "Efficient continuous wave and passively Q switched Er:$GdScO_3$ laser using Fe:ZnSe at 2.8 µm," Opt. Lett. **48**(8), 2118–2121 (2023).
16. W. Hou, H. Zhao, Z. Qin, *et al.*, "Spectroscopic and continuous-wave laser properties of Er:$GdScO_3$ crystal at 2.7 µm," Opt. Mater. Express **10**(11), 2730 (2020).
17. D. Hu, J. Dong, J. Tian, *et al.*, "Crystal growth, spectral properties and Judd-Ofelt analysis of Ho:$GdScO_3$ crystal," J. Lumin. **238**, 118243 (2021).
18. N. Li, J. Liu, R. You, *et al.*, "Spectroscopic characteristics and Judd-Ofelt analysis of Pr:$GdScO_3$ crystal," J. Lumin. **256**, 119599 (2023).
19. W. Wang, J. Tian, N. Li, *et al.*, "Crystal growth, polarization spectral analysis derived from the broadband emission from the $^1D_2$ level of Pr:$GdScO_3$ crystal," Opt. Mater. Express **12**(2), 468–478 (2022).
20. J. Li, G. Sun, Q. Zhang, *et al.*, "Effect of annealing atmosphere on the structure and spectral properties of $GdScO_3$ and Yb:$GdScO_3$ crystals," Acta. Phys. Sin. **71**(16), 164206 (2022).
21. Y. Zhang, S. Li, X. Du, *et al.*, "Yb:$GdScO_3$ crystal for efficient ultrashort pulse lasers," Opt. Lett. **46**(15), 3641–3644 (2021).
22. Y. Zhang, C. Huang, M. Xu, *et al.*, "Nd:$GdScO_3$ crystal: Polarized spectroscopic, thermal properties, and laser performance at 1.08 µm," Opt. Laser Technol. **167**, 109709 (2023).
23. Q. Song, N. Zhang, J. Liu, *et al.*, "Efficient continuous wave and broad tunable lasers with the Tm:$GdScO_3$ crystal," Opt. Lett. **48**(3), 640–643 (2023).
24. N. Zhang, Q. Song, J. Zhou, *et al.*, "44-fs pulse generation at 2.05 µm from a SESAM mode-locked Tm:$GdScO_3$ laser," Opt. Lett. **48**(2), 510–513 (2023).
25. J. A. Caird, S. A. Payne, P. R. Staver, *et al.*, "Quantum electronic properties of the $Na_3Ga_2Li_3F_{12}$:$Cr^{3+}$ laser," IEEE J. Quantum Electron. **24**(6), 1077–1099 (1988).


45.133.139.4 on 2024-05-14 03:03:12